

Shuttling Compiler for Trapped-Ion Quantum Computers Based on Large Language Models

Fabian Kreppel¹, Reza Salkhordeh¹, Ferdinand Schmidt-Kaler², and André Brinkmann³

¹Institute of Computer Science, Johannes Gutenberg University, Staudingerweg 9, 55128 Mainz, Germany

²Institute of Physics, Johannes Gutenberg University, Staudingerweg 7, 55128 Mainz, Germany

³Department of Computer Science, Saarland University, Saarland Informatics Campus, E1 1, 66123 Saarbrücken, Germany

Trapped-ion quantum computers based on segmented traps rely on shuttling operations to establish long-range connectivity between sub-registers. Qubit routing dynamically reconfigures qubit positions so that all qubits involved in a gate operation are co-located within the same segment, a task whose complexity increases with system size. To address this challenge, we propose a layout-independent compilation strategy based on large language models (LLMs). Specifically, we fine-tune pretrained LLMs to generate the required shuttling operations. We evaluate this approach on linear and branched one-dimensional architectures using quantum circuits of up to 16 qubits. Our results show that the fine-tuned LLMs generate valid shuttling schedules and, in some cases, outperform previous shuttling compilers by requiring approximately 15 % less shuttle overhead. However, results degrade as the algorithms increase in width and depth. In future, we plan to improve LLM-based shuttle compilation by enhancing our training pipeline using Direct Preference Optimization (DPO) and Gradient Regularized Policy Optimization (GRPO).

1 Introduction

Shuttling-based trapped-ion quantum computers [1–5] are currently limited by the number of qubits and the quality of gate operations. We are addressing the complexity that arises when a large number of qubits is routed efficiently for the execution of quantum algorithms.

For a scalable shuttle-based approach of a quantum computer, the quantum information is encoded in the internal states of individual ions, each of which represents a qubit; accordingly, we use the term *qubit* to refer to an ion throughout the paper. The qubits are confined in segmented microchip traps [6], where each

segment generates a localized potential well. By adjusting electrode voltages, trapping potentials can be dynamically reconfigured, enabling qubits to be shuttled between segments. Segments are either *storage segments*, where qubits are held, or *gate segments*. When two qubits are in the same gate segment, laser- or microwave-driven gate operations are executed. In accordance with the current maturity level of trapped-ion hardware, the number of available gate segments is still very limited [2,7]. In this work we restrict ourselves to a single gate segment, while the approach can be extended to a number of gate segments, which have been realized recently [5,8].

Current architectures arrange trap segments in a linear array [2,3,9,10] or in a racetrack loop [5], where each segment connects to two neighbors. Such designs limit scalability, as the number of qubits scales linearly with the physical size of the trap. Introducing junctions [11–14] increases connectivity, allowing segments to connect to multiple neighbors. Quantinuum has demonstrated this idea in their Helios architecture, where a ring-shaped storage region is connected to two linear legs via an X-shaped junction [8]. However, Helios contains only a single junction. Increasing the number of junctions would enable more complex topologies in the future, such as a two-dimensional quantum CCD [15].

Executing a quantum circuit requires a sequence of physical operations. The trap must be dynamically reconfigured using four fundamental shuttling operations:

- **Translation:** Moves the qubits to a neighboring segment.
- **Separation:** Splits two qubits from one segment into two different segments.
- **Merge:** Joins one qubit from the left and one from the right into one segment.
- **Swap:** Physically rotates within one segment, thus reversing the order of the qubits.

Shuttling operations introduce substantial time overhead [16]. As a result, error sources such as dephasing and noise-induced heating become more pronounced, and the shuttling process itself can further

Fabian Kreppel: f.kreppel@uni-mainz.de

Reza Salkhordeh: rsalkhor@uni-mainz.de

Ferdinand Schmidt-Kaler: fsk@uni-mainz.de

André Brinkmann: andre.brinkmann@uni-saarland.de

degrade gate fidelities through ion motional excitation and heating. Consequently, the number of shuttling operations must be minimized, highlighting the need for efficient compilation routines.

Compilation refers to the translation of a quantum circuit, which comprises abstract qubits and idealized gates, into a sequence of instructions executable on a specific trapped-ion device. This process starts out by decomposing gates into the device’s native gate set, then mapping qubits to trapped ions, and finally determining a *shuttling schedule* that defines an executable sequence of shuttling operations. The resulting schedule must adhere to the architecture of the processor while minimizing resource overheads such as operation time, qubit transport distance, etc.

Existing *shuttling compilers* compute valid qubit routing schedules by generating shuttling schedules tailored to specific architectures [3, 5, 7, 8, 17–25]. Due to the architectures growing complexity, designing separate heuristics for each layout becomes increasingly impractical.

We investigate large language models (LLMs) as a layout-independent alternative. LLMs can perform new tasks from textual instructions or a few demonstrations [26], making them well suited for learning shuttling behavior directly from examples.

In this work, we examine whether current LLMs can generate valid and efficient shuttling schedules and identify the challenges that arise when applying them to trapped-ion shuttling. We fine-tune LLaMA 3.2 [27], Qwen 3 [28], DeepSeek LLM [29], and Gemma 3 [30] on datasets derived from classical shuttling compilers for both linear [17, 18] and branched one-dimensional architectures with junctions [20]. We then compare the performance across multiple benchmark circuits. Moreover, we evaluate the ability to generalize to novel trap layouts.

Our compiler differs from machine-learning-based routing techniques developed for superconducting architectures [31–42]. While those methods primarily optimize SWAP placement and gate parallelism on fixed coupling graphs, our approach accounts for the hardware-specific characteristics of trapped-ion devices. Our work is the first to employ LLMs for compiling quantum circuits into shuttling schedules for trapped-ion quantum computers and to compare different LLMs for this task.

The remainder of this paper is structured as follows: [Sec. 2](#) reviews prior work on qubit routing and computing shuttling operations. [Sec. 3](#) presents our LLM-based approach, evaluated in [Sec. 4](#). Finally, [Sec. 5](#) summarizes our contributions and outlines future research directions.

2 Related Work

In logical quantum circuits with n qubits, each qubit can, in principle, interact with every other qubit, en-

abling the application of arbitrary unitary transformations on subsets of qubits. Such transformations are represented by complex-valued unitary matrices of dimension $2^N \times 2^N$, where $N \leq n$ denotes the number of qubits involved. In a real quantum computer, connectivity is limited by the device topology and only a limited subset of all possible unitaries is realizable by the hardware. To bridge this gap, quantum compilation stacks have been developed that can be adapted to multiple architectures, including Qiskit [43], $t|ket\rangle$ [44], and Cirq [45], as well as more general-purpose platforms such as PennyLane [46].

Due to the hardware characteristics of shuttling-based trapped-ion systems, shuttling compilers are a crucial component of the quantum compilation stack. Starting from a quantum circuit, they map qubits to ions and then derive shuttling schedules. While the minimal number of timesteps can be computed using Boolean satisfiability methods [47], most existing compilers employ heuristics to reduce the number of shuttling operations. Prior work includes design studies analyzing how architectural choices affect shuttling overhead [4, 48], as well as compilers targeting specific trap configurations [3, 5, 7, 8, 17–25]. However, all these existing approaches are tightly coupled to specific architectures.

Beyond single-trap systems, compilation has also been explored for distributed trapped-ion architectures, where multiple traps are connected via photonic interconnects that mediate quantum communication between nodes [49]. Such systems introduce additional scheduling and routing challenges, further highlighting the need for flexible compilation strategies that generalize across architectures.

3 Compiler

This section explains how we fine-tune LLMs to generate shuttling schedules for quantum circuit execution. The process comprises three phases: dataset generation, fine-tuning, and inference.

3.1 Dataset Generation

First, we require examples that illustrate how shuttling is performed. These examples are provided as *shuttling schedules*, as shown in [Fig. 1](#). Since the physical movements depend only on which qubits participate in each gate, rather than on the specific gate function, the gate functionality is omitted in this representation. Schedules can be generated in different ways, for example by constructing random sequences, by execution guided through a reward function, or by employing another (not necessarily optimized) compiler. The number of required schedules depends on the trap architecture, its size, and the number of qubits. Larger and more complex traps, as well as

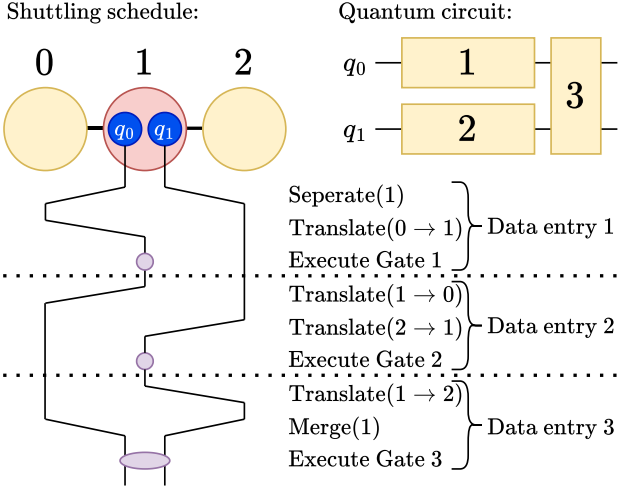


Fig. 1: Shuttling schedule of a quantum circuit with two qubits and three gates on a linear architecture consisting of three segments. Both qubits are initially located in gate segment 1. The lines indicate the qubit movements between the segments, while the purple dots denote gate executions. The executed shuttling operations are annotated alongside the lines. For dataset generation, the complete shuttling schedule is decomposed into multiple data entries, where each entry contains the shuttling operations between two consecutive gate executions, as indicated by the dotted lines.

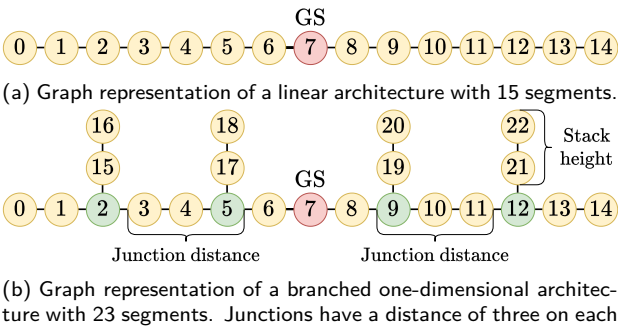


Fig. 2: Graph representations of ion-trap architectures. Red vertices denote gate segments (GS), yellow vertices denote storage segments, and green vertices denote junctions, which are the only vertices connected to more than two others. Numbers serve as unique vertex identifiers.

higher qubit counts, demand more shuttling operations per gate. This increases both the difficulty for the LLM to learn generating valid shuttling schedules and the amount of data required for fine-tuning.

The trap itself is modeled as a graph $G = (\mathcal{V}, \mathcal{E})$, where the vertex set \mathcal{V} represents the trap segments and the edge set \mathcal{E} represents physical connections between neighboring segments. Each vertex is assigned a unique natural number for identification. In this work, we focus on linear architectures and branched one-dimensional architectures with junctions, for which example graphs are shown in Fig. 2.

From the generated shuttling schedules, we construct two datasets: one for training and one for eval-

uation. The evaluation dataset is smaller and is used during training to assess model performance on unseen data. Both datasets consist of multiple data entries, obtained by disassembling the shuttling schedules as illustrated in Fig. 1. Each entry corresponds to the portion of the schedule between two gate executions. The first entry of a schedule starts with the initial trap state and the full quantum circuit and contains the shuttling sequence up to the first gate execution. After this gate is executed, the trap enters a new state and the gate is removed from the circuit. The remaining operations then describe how this new state evolves toward executing the next gate. The second entry covers the operations until that execution, and so on, until all gates are removed and the entire schedule is decomposed into data entries. When constructing datasets, it is also possible to mix schedules from different architectures so that a single LLM can be fine-tuned across them.

Each data entry follows the Alpaca format [50], consisting of an instruction and an output. Since the LLM can only process textual input, all required information is encoded as text.

3.1.1 Instruction

The instruction encodes all information the LLM requires to reason about the current trap configuration and valid operations. Since LLMs process purely textual input, all relevant information about the system must be encoded as text. For fine-tuning, the model input includes a graph-based description of the trap, its architectural constraints, the definitions of available shuttling operations, and the current trap state, including qubit locations, the circuit gates pending execution, and the shuttling operations permitted under that state.

The trap graph is defined by the sets of vertices and edges, where each vertex is identified by its unique natural number and each edge is represented by its incident vertices. Architectural constraints specify that each segment can hold a maximum number of qubits, which are arranged in a linear chain. Each qubit is assigned a position within this chain, allowing it to be uniquely referenced as a tuple $[v, p]$, where v denotes the vertex number and p the qubit's position in the chain.

In addition, the instruction specifies the quantum gates of the circuit, which must be executed on the given architecture. Each gate targets specific qubits and is assigned a unique natural number for identification. Due to architectural constraints, a gate is executable only if all involved qubits reside in the same gate segment, and this segment must not contain any additional qubits. The quantum circuit can be partitioned into layers such that the first layer contains only gates whose involved qubits have no predecessors and are executable once the corresponding qubits are in the gate segment, while gates in deeper layers have

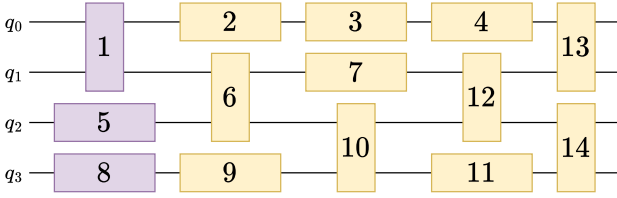


Fig. 3: Quantum circuit with four qubits and 14 gates. Purple gates form the first layer and are executable when their qubits are located in the gate segment, whereas yellow gates belong to deeper layers and are not yet executable. For each qubit, gates are numbered in ascending order to indicate their execution sequence.

at least one qubit with a predecessor and are therefore not yet executable. This layer-based division is illustrated in Fig. 3. For each qubit, the gate numbers are assigned in ascending order. To ensure the gate execution in the correct order, gates targeting the same qubit must be executed in numerical order, while gates acting on different qubits may be executed in any order. Finally, to link the circuit qubits with the qubits in the trap, all qubits in the gate descriptions are replaced by tuples $[v, p]$ of their corresponding position in the trap.

To modify the trap state, the LLM requires a description of the available shuttling operations. As outlined in Sec. 1, these include the four shuttling operations *Translate*, *Separate*, *Merge*, and *Swap*, as well as gate execution. While gates can only be executed on the gate segments, depending on the hardware, separation, merging, and swapping may also be permitted on storage segments or a subset thereof.

In segmented trapped-ion architectures, junctions are formed by the intersections of electrodes, enabling qubits to be routed between different linear sections. Qubits must pass through junctions without stopping, and reversing direction within a junction is infeasible because the electric fields are engineered for unidirectional traversal rather than oscillatory motion [13, 51]. In particular, *Separate*, *Merge*, *Swap*, and gate execution cannot be performed on junction vertices, which must remain empty throughout execution. Furthermore, for *Separate* and *Merge*, the adjacent vertices involved must not be junctions. The operations are formally defined as follows:

- **Translate:** Move all qubits from a vertex $v \in \mathcal{V}$ to a neighboring vertex $u \in \mathcal{V}$, provided that $\{v, u\} \in \mathcal{E}$ and u is empty. After translation, v becomes empty. To prevent qubits from being moved to and from a junction without first being moved to another storage segment, an additional rule applies: if u is a junction, a translation from u to v cannot be reversed until a subsequent translation from u to another neighbor $w \neq v$ has been executed.
- **Separate:** Let $v \in \mathcal{V}$ be a vertex eligible for sep-

aration, containing $n \geq 2$ qubits, with empty neighbors $v-1$ and $v+1$. The qubits at positions $0, \dots, \lceil \frac{n}{2} \rceil$ in the qubit chain of v are moved to $v-1$, while the remaining qubits are moved to $v+1$. After separation, v is empty.

- **Merge:** Let $v \in \mathcal{V}$ be an empty vertex eligible for merging, with neighbors $v-1$ and $v+1$ containing m and n qubits, respectively, such that $m+n$ does not exceed the maximum segment capacity. The qubits from $v-1$ and $v+1$ are moved into v , where positions $0, \dots, m-1$ are occupied by the qubits from $v-1$ and positions $m, \dots, m+n-1$ by the qubits from $v+1$. After merging, $v-1$ and $v+1$ are empty.
- **Swap:** Let $v \in \mathcal{V}$ be a vertex eligible for swapping, containing at least two qubits. Reverse the order of the qubit chain in v .
- **Execute Gate:** Perform the quantum gate in the gate segment, once all previously defined execution conditions are satisfied.

After specifying all rules to the LLM, the overall goal is defined: execute all gates using the minimal number of operations. To accomplish this, the LLM must also be aware of the current trap state. Accordingly, the instruction includes four enumerations:

- 1) **Qubit positions:** All qubits in the trap, each represented by its position tuple $[v, p]$ as described above.
- 2) **First-layer gates:** All gates in the first layer of the circuit that are executable when their corresponding qubits reside in the gate segment, along with the tuples of the qubits they act on.
- 3) **Deeper-layer gates:** Gates in deeper layers that are not yet executable, along with the tuples of the qubits they act on. To keep the focus on near-term execution, this list includes only the gates that become executable next, rather than all remaining gates in the circuit.
- 4) **Allowed shuttling operations:** All shuttling operations currently valid for the given trap state, allowing the LLM to select a valid first step without ambiguity.

The instruction concludes by defining the task for the LLM: generate a shuttling sequence that enables the execution of one of the first-layer gates, contributing to the overall goal. After each operation, the LLM should also provide the updated qubit positions, the list of first-layer gates with the updated position tuples of the qubits, and the new set of allowed shuttling operations. Requiring these additional outputs at each step supports the LLM to reason carefully about the current state and the implications of each operation.

3.1.2 Output

To learn, the LLM needs examples of expected shuttling sequences during the training phase that solve the task given in the instruction. Therefore the output contains the part of the previous generated shuttling schedule that shows how one of the first-layer gates can be executed from the given state. As long as not all requirements are fulfilled to execute one of the gates, usually multiple shuttling operations are required. The number of operations depends on the size of the trap and the number of qubits used. The reason is that with increasing trap size and qubit number, more shuttling operations are required to reconfigure the trap segments so that the trap is in a valid state for a gate execution.

The output begins with the first shuttling operation which is to be executed. This includes the updated qubit positions, the first-layer gates, and the new allowed shuttling operations. This information helps the LLM to learn which changes happen with the executed shuttling operation. Afterwards, the output contains the next shuttling operation based on the new state. This continues until the operation “Execute Gate” indicates that the ions are arranged such that a first-layer gate can be executed.

3.2 Fine-tuning with Axolotl

After dataset preparation, we fine-tune pre-trained LLMs from Huggingface [52] to compute shuttling schedules. For this, we fine-tune with *Axolotl* [53], which provides seamless compatibility with Huggingface models. *Axolotl* supports various training approaches, including full fine-tuning, Low-Rank Adaptation (LoRA) [54], and Quantized LoRA (QLoRA) [55]. Since LoRA and QLoRA did not yield good results (see Sec. 3.4), we performed full fine-tuning of the LLM. Furthermore, *Axolotl* offers performance optimizations such as multipacking [56], FlashAttention 2 [57], sequence (context) parallelism [58], and multi-GPU training with DeepSpeed [59], which we describe in more detail below.

3.2.1 Performance Optimizations

To minimize resource requirements and enable fine-tuning on as few GPUs as possible, it is essential to reduce memory usage and parallelize execution. We achieve this with *DeepSpeed*, employing the Zero Redundancy Optimizer (ZeRO) at optimization level 3 [60] to accelerate and distribute fine-tuning [61]. In this setting, 16-bit model parameters are partitioned across GPUs, while DeepSpeed manages parameter partitioning and collection during forward and backward passes. To further reduce memory consumption, we use `bfloat16` as the 16-bit floating-point format. Additionally, we apply ZeRO Offloading [62], which transfers optimizer states, as well as model param-

eters and gradients when inactive, to the host CPU and RAM.

The data entries in our datasets vary considerably in length due to differing output sizes, which depend on the number of shuttling operations required to execute one of the first-layer gates. While in some cases, a gate can be executed directly within the current trap configuration, other cases require complex shuttling operations, producing significantly longer outputs. Since fine-tuning requires sequences of uniform length, shorter sequences are padded with special tokens. To avoid excessive padding to match the longest sequence, we apply *multipacking*, which enables training on multiple shorter entries simultaneously, provided the combined length does not exceed the model’s context window. To efficiently process longer sequences, we employ *FlashAttention 2*, an optimized attention mechanism that improves memory efficiency and accelerates training, thereby allowing for longer sequence lengths. For cases where individual sequences exceed the VRAM capacity of a single GPU, we use *sequence parallelization*. This approach relies on blockwise ring attention [63], which enables distributed computation of self-attention and feedforward layers across multiple GPUs, while overlapping communication and computation to minimize overhead.

Moreover, because each instruction in our dataset specifies a problem and its context, while the corresponding output provides a step-by-step solution, we compute the loss exclusively on the output. This encourages the model to generalize solutions rather than memorize instructions.

The fine-tuning process is divided into two phases: pre-processing and training. These phases are managed automatically by *Axolotl* upon submission of a YAML configuration file, which specifies, among other parameters, the performance optimization settings and the file paths to the model, training and evaluation datasets, and the DeepSpeed configuration. The latter defines all DeepSpeed-related settings.

In the following, we discuss the two fine-tuning phases in more detail.

3.2.2 Pre-processing

The pre-processing phase prepares the dataset to streamline subsequent training. During this phase, *Axolotl* validates the YAML configuration file, ensuring that all required libraries are installed and that the selected optimizations are compatible. It then initializes the tokenizer and parses and formats both the training and evaluation datasets. Since the loss is computed exclusively on the output, instruction tokens are masked. With *multipacking*, multiple data entries are concatenated up to a defined maximum length with respect to the correct loss mask. The processed dataset, including tokenized inputs, loss masks,

and associated metadata, is saved in Apache Arrow format for use during training.

3.2.3 Training

During the training phase, *Axolotl* coordinates the various optimization strategies. It loads the model, tokenizer, and pre-processed datasets using Huggingface’s `datasets` library and distributes them according to the selected optimizations. When loading the model, *Axolotl* integrates the memory-efficient attention mechanism from Flash Attention 2. It also configures Huggingface’s `Trainer` from its `transformer` library with the required parameters and connects it to DeepSpeed. While DeepSpeed handles memory optimizations and parallelization, the `Trainer` manages the training loop, which loads micro-batches of tokenized data. To conserve memory, each iteration uses a batch size of one; the forward pass computes the loss on the output, which is backpropagated to calculate gradients. We use gradient accumulation over eight batches to mitigate gradient noise and to improve convergence despite the small batch size. The accumulated gradients are applied by the AdamW optimizer [64] to update the network weights. In addition to training, the `Trainer` handles logging, evaluation at regular intervals, and checkpointing. We fine-tune the model for a single epoch on the training dataset. Performing a single epoch rather than multiple ones enables us to leverage larger datasets, so the model encounters a greater variety of examples. Upon completion, the fine-tuned model is saved for inference.

3.3 Inference with *vLLM*

After fine-tuning, the model is deployed for inference using *vLLM* [65], which provides efficient multi-GPU support. Its *PagedAttention* mechanism optimizes memory management of attention keys and values, thereby reducing overhead. Since *vLLM* is fully compatible with Huggingface models, it integrates seamlessly with our fine-tuned model. For inference, we launch a local *vLLM* server, which automatically loads the model and its tokenizer. The server exposes an OpenAI-compatible API accepting JSON-formatted HTTP requests. Each request contains an instruction in the same format as the training data, together with the maximum number of tokens to generate. Since outputs can be lengthy depending on the required operations, we set this limit to 29,000 tokens. The server returns the response in JSON format, from which we extract the generated output. To obtain clean text, special tags such as `<think>` are removed.

Each request to the *vLLM* server produces a single output describing the shuttling operations required to execute one of the first-layer gates. Thus, multiple requests are necessary to construct a complete

shuttling schedule. Since outputs may include invalid operations inconsistent with the trap architecture or current state, we developed a Python script to automate schedule generation and validation. The script tracks both the qubit positions in the trap and the remaining, not-executed gates of the circuit. At initialization, it loads the quantum circuit, heuristically determines an initial qubit placement on the trap graph, and identifies first-layer gates, deeper-layer gates, and allowed shuttling operations. Using this information, it constructs an instruction in the same format as the training data and submits it to the *vLLM* server.

The returned output is then validated by checking whether all operations are consistent with the architectural rules and whether at least one first-layer gate has been successfully executed. If the output is valid, redundant translations, such as unnecessary back-and-forth movements of qubits between segments, are removed to reduce the overall operation count. Similarly, consecutive merges and separations on the same qubits without intermediate operations, as well as successive swap operations, are eliminated. Afterwards, the script updates the qubit positions, removes the executed gate from the circuit, and generates the next instruction based on the updated state before resubmitting it to the *vLLM* server. This iterative process continues until all gates have been executed. If an invalid output is produced, the same instruction is resubmitted to the *vLLM* server to obtain a valid result. To prevent infinite loops, the procedure terminates if ten consecutive invalid outputs occur for the same instruction.

In principle, it would also be possible to request multiple outputs from the *vLLM* server at once, validate and post-process them, and then select the valid output with the fewest operations. However, we chose to generate and evaluate only one output at a time. The reasons are twofold: first, depending on the complexity of the shuttling operations required to perform one of the first-layer gates, generating each output may take over one minute; and second, always selecting the locally optimal output with the fewest operations does not guarantee a globally minimal shuttling schedule. The process may converge to a local minimum, requiring additional operations to escape. Avoiding this would require exploring multiple valid continuations for each output over several steps and then selecting the output that starts the path with the lowest total number of operations. While such a lookahead strategy could reduce the overall number of operations, its runtime would grow exponentially with the number of steps.

In summary, the complete compilation flow of our compiler is illustrated in Fig. 4.¹

¹The datasets, training scripts, and trained models are available from the authors upon request.

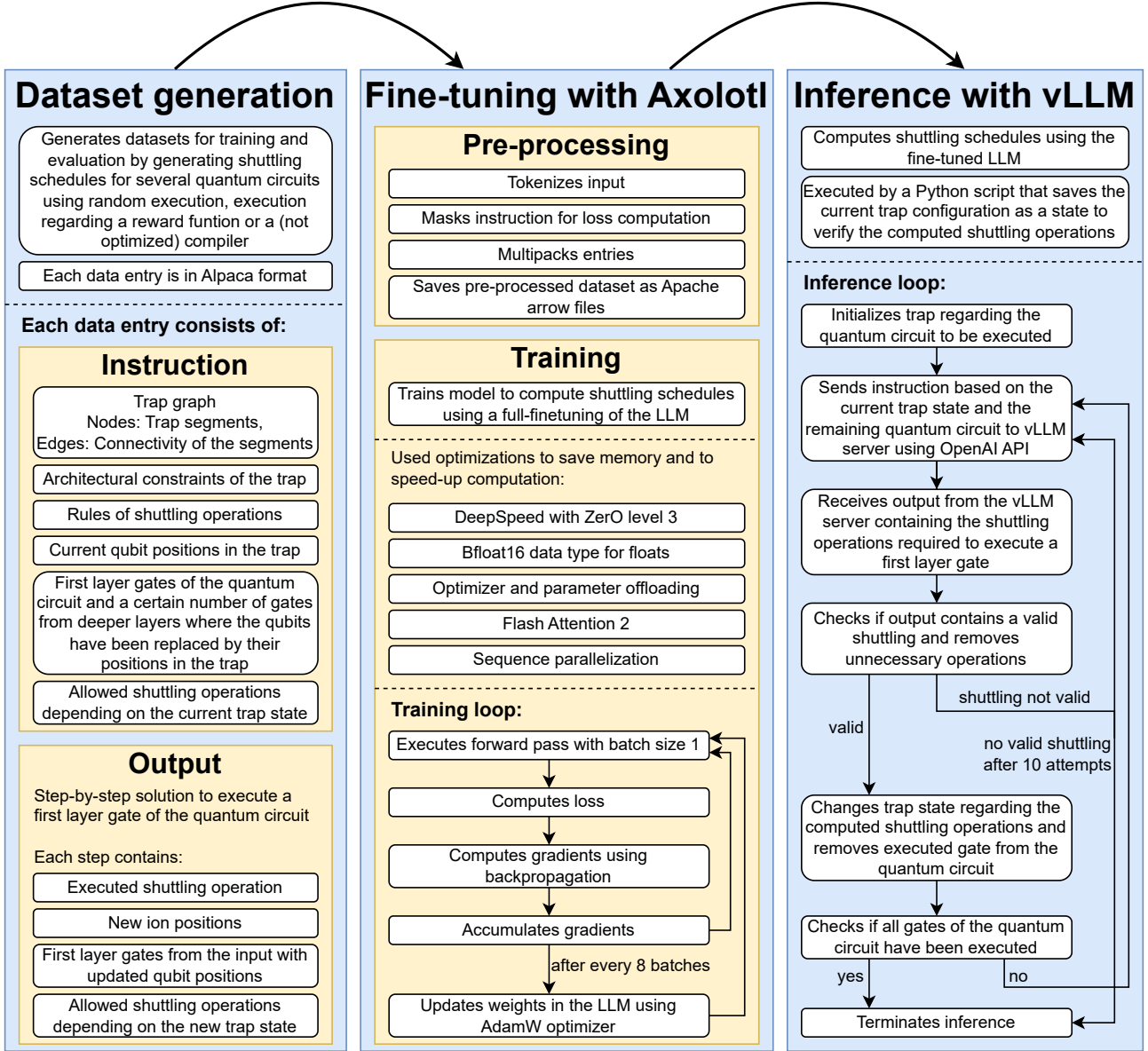


Fig. 4: Overview of the three phases of our compiler. We first generate training and evaluation datasets in Alpaca format, where each entry consists of an instruction and its corresponding output. These datasets are then used to fine-tune an LLM with *Axolotl*, which involves pre-processing and training. Finally, the fine-tuned model is deployed for inference to compute shuttling schedules by submitting instructions to a *vLLM* server.

3.4 Alternative Approaches and Challenges

In addition to the fine-tuning strategy described above, we explored several alternative approaches to reduce data complexity and resource requirements. While these methods provided insights, they did not yield satisfactory results in practice.

First, to reduce the length of the data entries, we attempted to reduce the output size in the training and evaluation datasets by splitting each shuttling operation into a separate entry. In this setup, the first entry contained the same state information as the original instruction but produced only the first shuttling operation as output. After applying this operation, the qubit positions were updated, and the new state was

used in the instruction of the next entry, whose output contained the second shuttling operation. This is continued until all operations of the original entry were separated. For the example in Fig. 1, this would result in nine entries instead of three. While this approach reduced the size of individual entries, it substantially increased their total number. Moreover, during inference with models fine-tuned on such datasets, the LLM often selected randomly among the valid shuttling operations. Although the chosen operations were valid, they did not necessarily advance the execution of the quantum circuit.

Second, instead of limiting the instruction to the first-layer gates and a subset of deeper-layer gates, we included the entire remaining circuit in OpenQASM

format [66, 67], along with a mapping from qubits to their positions in the trap. While this approach has much longer state descriptions, it also introduced a critical drawback: the LLM was unable to reliably identify the first-layer gates and frequently generated shuttling operations that targeted arbitrary, and often deeper-layer, gates.

Finally, we evaluated parameter-efficient fine-tuning methods such as LoRA and QLoRA, which restrict training to the linear layers and thereby reduce the number of trainable parameters and VRAM requirements. However, models fine-tuned with LoRA or QLoRA tended to generate step-by-step reasoning instead of directly producing the expected output format. These derivations often failed to fully account for the rules governing shuttling operations, leading to incorrect schedules. In addition, the deviation from the expected output format made it more difficult to automatically extract the relevant shuttling operations.

Given these limitations, we focused on the main fine-tuning approach described above.

4 Evaluation

This section evaluates the performance and generalization capabilities of our LLM-based shuttling compiler. We fine-tuned several LLMs using shuttling examples from both the linear architecture and the branched one-dimensional architecture with junctions, and then assessed how well the resulting models generate valid and efficient shuttling schedules. The evaluation includes multiple benchmark circuits compiled for the two architectures seen during training as well as three previously unseen layouts, shown in Fig. 5. The following subsections describe the experimental setup and present the results.

4.1 Setup

In the following, we first describe the setup used for fine-tuning the models and then outline the setup employed for inference with the fine-tuned LLMs.

4.1.1 Fine-tuning

We performed fine-tuning on a single node equipped with eight H100 GPUs, each providing 80 GB of VRAM. Therefore, first we generated separate training and evaluation datasets containing examples for both the linear and the branched one-dimensional architectures with junctions. In both architectures, a single gate segment was used, and the *separate*, *merge*, and *swap* operations were executable only within this segment. This configuration imposes the strongest execution constraints, making it the most challenging setup for the LLMs to learn. The trap graphs were designed such that the number of storage segments on

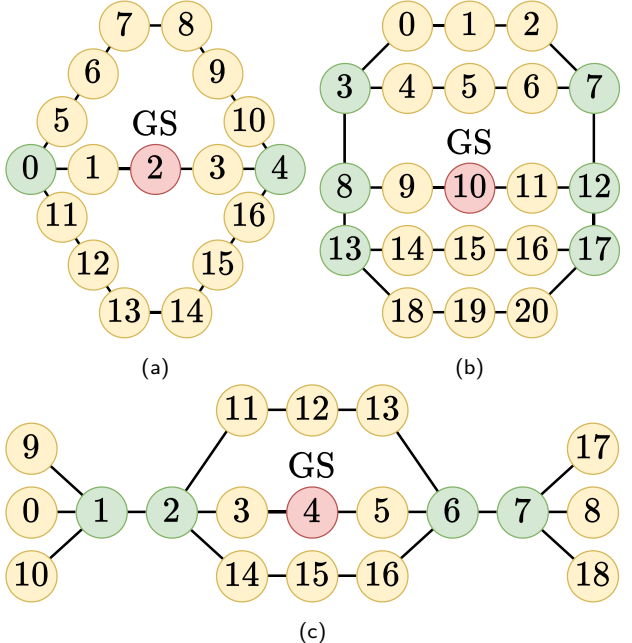


Fig. 5: Graph representations of ion-trap architectures used to evaluate the generalization capabilities of the fine-tuned LLMs on previously unseen layouts. Architectures (a) and (b) feature three-way junctions, while architecture (c) contains four-way junctions (green). For each layout, the number of storage vertices (yellow) was scaled to match the qubit count of the respective test circuit. GS (red) indicates the segment, where quantum gates are executed.

each side of the gate segment matched the number of qubits in the circuit.

For the linear architecture, the number of qubits was varied between 2 and 16. For the junction architecture, the number of qubits ranged from 3 to 16, and we additionally varied the *stack depth*, specifying the number of storage segments per stack, and the *junction distance*, defining the spacing between the junctions on each side of the gate segment, as illustrated in Fig. 2b. In the following, we denote the stack depth by s and the junction distance by d . Due to hardware limitations, we restricted the datasets to circuits of these sizes, as larger circuits would require more complex shuttling patterns and, consequently, additional VRAM and GPUs for fine-tuning.

Shuttling schedules were generated using the compilers [17] and [20] for the linear and branched architecture, respectively. The underlying quantum circuits were randomly generated with Qiskit [43], containing single- and two-qubit gates with a depth of five. These circuits were then compiled into a trapped-ion-compatible format [68].

For the linear architecture, 120 shuttling schedules per qubit count were included in the training dataset and 30 in the evaluation dataset. For the junction architecture, eight schedules per trap design and qubit count were used for training and two for evaluation. Both datasets contained approximately equal propor-

tions of examples from each architecture and were automatically shuffled by Axolotl prior to fine-tuning to ensure uniform data distribution.

Due to the hardware constraints and the size of the dataset entries, model sizes were limited to 50 GB, preventing us from fine-tuning large models such as DeepSeek V3 [69], DeepSeek R1 [70], or LLaMA 4 [71]. Within these limits, we fine-tuned a variety of models, including LLaMA 3.2 with 3 billion parameters [27], Qwen 3 with 4 and 14 billion parameters [28], DeepSeek LLM with 7 billion parameters [29], and Gemma 3 with 27 billion parameters [30].

In addition, we attempted to fine-tune GPT-OSS with 20 billion parameters [72], which required replacing DeepSpeed with FSDP2 [73]. However, we were unable to evaluate this model on the test set because it consistently produced invalid responses after finetuning: the first one or two shuttling operations were always truncated, making it impossible to construct a valid schedule.

4.1.2 Inference

For inference, we evaluated LLaMA, Qwen, and DeepSeek on a single A100 GPU with 40 GB VRAM on the Mogon NHR cluster of Johannes Gutenberg University. Due to its larger model size, Gemma was evaluated on a single A100 GPU with 80 GB VRAM on the Mogon KI cluster. As test circuits for compilation with the fine-tuned LLMs, we selected three of the 153 circuits from the library of [74], which have been used in prior work [20, 68, 75, 76]: *4mod5-bdd_287* (7 qubits, 106 gates), *mini_alu_305* (10 qubits, 263 gates), and *cnt3-5_179* (16 qubits, 230 gates). The gate counts refer to the circuits after compilation using [68]. We chose these circuits because they span different qubit counts and, within the library, have the lowest gate counts for their respective qubit numbers. Since each request to the *vLLM* server returns the shuttling operations for a single gate, inference time is strongly influenced by the number of gates. Thus, selecting circuits with minimal gate counts kept the benchmarks manageable while still allowing us to evaluate performance across multiple qubit regimes.

For each circuit, we used the fine-tuned models to generate shuttling schedules for the linear architecture and for 10 (*4mod5-bdd_287*), 18 (*mini_alu_305*), and 29 (*cnt3-5_179*) branched architectures, each defined by different combinations of stack depth and junction distance. To assess generalization, we additionally evaluated the models on the previously unseen architectures shown in Fig. 5. As in the training data, each graph contained a single gate segment, and the *separate*, *merge*, and *swap* operations were executable only within that segment. We also evaluated the stochastic behavior of the models by varying T , which controls how deterministic the output is. Lower T yields more deterministic outputs, and

with $T = 0.0$ the model becomes fully deterministic. Higher T increase the level of randomness in the generated outputs. To balance determinism and variability, we evaluated each model–circuit–architecture combination at $T = 0.7$ and $T = 1.0$. For each configuration, we performed ten runs and limited the runtime to eight hours per run.

4.2 Results

This subsection presents the results of our evaluation. The minimal number of shuttling operations required by the schedules generated by LLaMA, Qwen-4B, Qwen-14B, DeepSeek, and Gemma is summarized in Tab. 1, together with the corresponding values from the baseline compilers [17, 20]. If a model failed to produce a valid schedule, the table reports how many gates were executed before the generation process became invalid. Since schedule generation on the architectures shown in Fig. 5a and Fig. 5b failed at early stages, these architectures are not included in the table.

Additional statistics on the generation process are provided in Tab. 2, including the number of required retries and the number of response tokens. We measure the number of generated tokens rather than runtime because token counts are hardware-independent and commonly used as a billing metric for LLMs [77]. In contrast, runtime depends heavily on hardware factors such as GPU type, the number of GPUs used, their distribution across cluster nodes, and the intra- and inter-node interconnects. For each configuration, we report both the token count of the final valid schedule, which excludes retries, and the total tokens generated across all attempts, including failed ones. The table also indicates, for each junction architecture, the number of configurations that produced valid schedules and how many of these schedules required fewer shuttling operations than the baseline compiler with the same configuration.

We now present the results obtained by the LLMs for the linear and branched one-dimensional architectures with junctions, comparing them with each other and with the baseline compilers [17, 20]. Subsequently, in Sec. 4.2.2, we evaluate the performance of the LLMs on the previously unseen architectures depicted in Fig. 5.

4.2.1 Linear and branched one-dimensional architectures

For *4mod5-bdd_287* on the linear architecture, DeepSeek, LLaMA at $T = 0.7$, and Qwen-4B at $T = 1.0$ produced schedules requiring fewer operations as compared with the baseline, whereas Qwen-14B and Gemma consistently generated schedules with higher overhead. The best result was obtained by Qwen-4B at $T = 1.0$, reducing the operation effort by 15 %,

Tab. 1: Operation effort of shuttling schedules generated by LLaMA, Qwen, DeepSeek, and Gemma with different T values compared to the baseline [17, 20]. For each model, only the run with the fewest operations is reported. For the junction architecture, we list only the best-performing configuration and specify the corresponding stack depth s and junction distance d as (s, d) . If none of the ten runs succeeded, the entry is marked as “failed”, with the number of successfully executed gates shown in parentheses. If all junction configurations failed, the table reports the configuration that completed the most gates before failure.

Architecture	Baseline	LLaMA 3.2-3B		Qwen 3-4B		Qwen 3-14B		DeepSeek-7B		Gemma 3-27B	
		$T = 0.7$	$T = 1.0$	$T = 0.7$	$T = 1.0$	$T = 0.7$	$T = 1.0$	$T = 0.7$	$T = 1.0$	$T = 0.7$	$T = 1.0$
Circuit: 4mod5-bdd_287, 7 qubits, 106 gates											
Linear	607	559	653	1,071	517	842	701	598	543	700	825
Best junction	482 (1, 3)	506 (2, 1)	464 (2, 3)	547 (2, 2)	537 (1, 2)	518 (2, 2)	545 (2, 2)	541 (3, 1)	566 (2, 1)	533 (2, 3)	521 (2, 2)
Fig. 5c	failed (12)	569	failed (23)	failed (33)	failed (52)	failed (26)	failed (4)	failed (4)	failed (7)	failed (16)	failed
Circuit: mini_alu_305, 10 qubits, 263 gates											
Linear	2,390	failed (106)	failed (161)	failed (165)	3,124	failed (95)	failed (86)	failed (123)	failed (98)	failed (70)	failed (75)
Best junction	1,624 (2, 1)	1,791 (2, 3)	1,809 (2, 2)	failed (168) (4, 2)	2,776 (5, 1)	failed (85) (3, 2)	failed (70) (1, 3)	failed (67) (4, 2)	failed (69) (2, 4)	failed (95) (4, 2)	failed (126) (5, 1)
Fig. 5c	failed (38)	failed (48)	failed (19)	failed (13)	failed (15)	failed (15)	failed (0)	failed (0)	failed (16)	failed (13)	failed
Circuit: cnt3-5_179, 16 qubits, 230 gates											
Linear	3,467	failed (142)	failed (146)	failed (103)	failed (118)	failed (80)	failed (98)	failed (63)	failed (59)	failed (88)	failed (43)
Best junction	1,716 (2, 1)	2,435 (1, 1)	2,017 (3, 1)	failed (140) (10, 1)	failed (111) (3, 2)	failed (64) (6, 3)	failed (59) (6, 1)	failed (44) (4, 3)	failed (49) (5, 4)	failed (56) (4, 3)	failed (53) (4, 4)
Fig. 5c	failed (12)	failed (16)	failed (7)	failed (9)	failed (4)	failed (3)	failed (5)	failed (5)	failed (5)	failed (7)	failed

indicating that the smaller Qwen model performs better than the larger one on this architecture. However, Qwen-4B also yielded the worst result at $T = 0.7$, requiring 76% more operations than the baseline. Across all models, 2 to 26 retries were needed, and valid schedules contained between 60,440 and 143,057 response tokens. When retries were included, token counts increased by up to a factor of 6.2. Notably, the best-performing Qwen-4B run also produced the smallest final token count, but its high number of 26 retries led to the largest overall increase when considering all generated tokens.

For the junction architecture, LLaMA produced valid schedules for all ten tested configurations and, at $T = 1.0$, outperformed the baseline in three cases. Qwen-14B produced valid schedules for all configurations except $s = 1, d = 4$ and surpassed the baseline for $s = 5, d = 1$ at $T = 0.7$ and $T = 1.0$. Qwen-4B generated valid schedules for eight configurations and outperformed the baseline for the same configuration as Qwen-14B, but only at $T = 1.0$. Gemma yielded valid schedules for seven configurations at $T = 1.0$ and five at $T = 0.7$, while DeepSeek produced valid schedules for only five configurations at $T = 1.0$ and one at $T = 0.7$; neither model surpassed the baseline. LLaMA’s best result, obtained for $s = 2, d = 3$ at $T = 1.0$, required 4% fewer operations than the best baseline configuration $s = 1, d = 3$ and needed only a

single retry, leading to similar token counts with and without retries. In contrast, the best results of the other models required 7% to 12% more operations than the baseline and involved substantially more retries, ranging from 9 to 40. This resulted in token counts up to 5.1 times higher when retries were included.

As the number of qubits increases, generating valid schedules becomes substantially more challenging. While LLaMA was still able to produce valid schedules for several junction configurations on both larger benchmark circuits, Qwen-4B generated a valid schedule only for the linear architecture and a single junction configuration of *mini_alu_305*. However, Qwen-14B, DeepSeek, and Gemma failed to generate any complete schedules for the two larger circuits.

For *mini_alu_305* on the linear architecture, Qwen-4B at $T = 1.0$ was the only model to produce a complete schedule, requiring 3,124 shuttling operations, corresponding to a 31% increase over the baseline. The resulting schedule contained 555,430 tokens, and its computation required 33 retries, increasing the total number of generated tokens by a factor of 7.7. All other models, including Qwen-4B at $T = 0.7$, failed to generate a complete schedule for this circuit. The increasing difficulty can be attributed to the larger number of qubits, which makes trap reconfiguration more complex and often necessitates recur-

Tab. 2: Statistics for the best runs reported in Tab. 1. For each run, we report the number of retries and the number of response tokens required to generate the complete shuttling schedule. The token count is given once without retries, where only the tokens of the final valid solution are included, and once with retries, where all tokens generated during invalid attempts are also counted. For the junction architecture, we additionally report how many configurations produced valid schedules and, among those, how many achieved fewer operations than the baseline compiler on the same configuration.

Architecture	Parameter	LLaMA 3.2-3B		Qwen 3-4B		Qwen 3-14B		DeepSeek-7B		Gemma 3-27B	
		$T = 0.7$	$T = 1.0$	$T = 0.7$	$T = 1.0$	$T = 0.7$	$T = 1.0$	$T = 0.7$	$T = 1.0$	$T = 0.7$	$T = 1.0$
Circuit: 4mod5-bdd_287											
Linear	Retries	9	9	19	26	2	17	5	15	17	15
	Resp. toks w/o retries	61,026	78,302	143,057	60,440	99,779	85,658	75,542	72,603	85,898	103,769
	Resp. toks w/ retries	183,015	282,865	465,466	372,417	179,779	416,445	102,256	172,337	250,340	271,816
Best junction	Retries	3	1	17	15	22	14	28	40	9	25
	Resp. toks w/o retries	65,514	56,347	79,480	78,681	98,207	80,583	90,623	93,918	76,700	73,839
	Resp. toks w/ retries	74,007	57,120	238,377	226,940	364,637	176,697	463,023	389,144	169,306	239,441
Succ. junction confs.		10/10	10/10	8/10	8/10	9/10	9/10	1/10	5/10	5/10	7/10
Confs. outperf. class.		0/10	3/10	0/8	1/8	1/9	1/9	0/1	0/5	0/5	0/7
Fig. 5c	Retries	—	36	—	—	—	—	—	—	—	—
	Resp. toks w/o retries	—	67,745	—	—	—	—	—	—	—	—
	Resp. toks w/ retries	—	228,928	—	—	—	—	—	—	—	—
Circuit: mini_alu_305											
Linear	Retries	—	—	—	33	—	—	—	—	—	—
	Resp. toks w/o retries	—	—	—	555,430	—	—	—	—	—	—
	Resp. toks w/ retries	—	—	—	1,251,636	—	—	—	—	—	—
Best junction	Retries	26	29	—	58	—	—	—	—	—	—
	Resp. toks w/o retries	401,431	392,065	—	629,391	—	—	—	—	—	—
	Resp. toks w/ retries	725,633	766,859	—	2,187,631	—	—	—	—	—	—
Succ. junction confs.		15/18	11/18	0/18	1/18	0/18	0/18	0/18	0/18	0/18	0/18
Confs. outperf. class.		1/15	2/11	—	0/1	—	—	—	—	—	—
Circuit: cnt3-5_179											
Best junction	Retries	27	104	—	—	—	—	—	—	—	—
	Resp. toks w/o retries	646,571	564,133	—	—	—	—	—	—	—	—
	Resp. toks w/ retries	1,415,626	2,592,367	—	—	—	—	—	—	—	—
Succ. junction confs.		1/29	2/29	0/29	0/29	0/29	0/29	0/29	0/29	0/29	0/29
Confs. outperf. class.		0/1	0/2	—	—	—	—	—	—	—	—

sive shuttling operations. Consequently, the models frequently reach trap configurations from which continuing schedule generation becomes infeasible. Moreover, since our compiler generates schedules gate after gate, the likelihood of encountering unrecoverable configurations grows with circuit depth. Nevertheless, the models were able to execute between 70 and 165 of the 263 gates, indicating that substantial partial progress remains achievable. Among these models, Gemma performed worst, whereas LLaMA executed more than 100 gates before failing.

On the junction architecture, Gemma, Qwen-14B, and DeepSeek again failed to complete any schedule,

executing at most 126, 85 and 69 gates, respectively. Qwen-4B produced a valid result only for the configuration $s = 5, d = 1$ at $T = 1.0$, requiring 71 % more operations than the best baseline configuration $s = 2, d = 1$ with 1,624 operations. This run required 58 retries, increasing the total number of generated tokens to 3.5 times the size of the final schedule. Among the failed runs, Qwen-4B at $T = 0.7$ performed best, executing 168 gates before failure for the configuration $s = 4, d = 2$. However, LLaMA performed substantially better: of the 18 tested configurations, 15 at $T = 0.7$ and 11 at $T = 1.0$ yielded valid schedules, with one and two of these, respectively, outperform-

ing the baseline. Unlike the linear architecture, where LLaMA failed, the presence of stacks in the junction architecture provides intermediate storage locations that simplify reconfiguration and reduce the need for recursive operations. Relative to the best baseline configuration, LLaMA achieved the best results for the configurations $s = 2, d = 3$ at $T = 0.7$ and $s = 2, d = 2$ at $T = 1.0$ requiring only 11 % more operations. These runs required 26 and 29 retries, respectively, roughly doubling the number of generated tokens compared to the final schedules.

For *cnt3-5_179*, none of the models generated a complete schedule on the linear architecture. LLaMA executed more than 140 gates before failing, whereas Qwen-4B failed after over 100 gates and Qwen-14B completed up to 98 gates. DeepSeek failed after approximately 60 gates. Gemma’s performance strongly depended on T : at $T = 0.7$ it failed after executing 88 gates, while at $T = 1.0$ it executed only 43 gates before failing. Notably, LLaMA’s performance indicates that, in principle, shuttling schedules for 16-qubit circuits are attainable, although robustness remains a limiting factor.

On the junction architecture, both Qwen models, Gemma and DeepSeek failed for all configurations. While Qwen-4B could execute up to 140 gates, only about 60 gates for Qwen-14B, 55 for Gemma, and 45 for DeepSeek could be executed. As for *mini_alu_305*, LLaMA also performed best here. Out of 29 tested configurations, LLaMA produced valid schedules for one at $T = 0.7$ and two at $T = 1.0$, but none outperformed the baseline. The best baseline configuration $s = 2, d = 1$ required 1,716 operations, whereas LLaMA’s best result achieved with configuration $s = 3, d = 1$ at $T = 1.0$ required 18 % more operations. This run required 104 retries, increasing the number of generated tokens by a factor of 4.6 relative to the final schedule.

4.2.2 Unseen architectures

In addition to linear and branched one-dimensional architectures with junctions, we evaluated the generalization capabilities of the fine-tuned LLMs on the unseen architectures shown in Fig. 5.

The layouts in Fig. 5a and Fig. 5b feature three-way junctions, similar to the branched architectures used during training. For all those architectures, none of the models generated a valid shuttling schedule for any of the evaluated circuits. While on the first architecture, all models failed immediately during schedule generation, on the second one, the models were able to execute up to four gates before failing.

In contrast, one model successfully generated a valid schedule for the four-way junction architecture shown in Fig. 5c for the circuit *4mod5-bdd_287*. LLaMA at $T = 0.7$ produced a valid schedule with 569 shuttling operations but required 55 retries, increasing the total token count by a factor of 6.0 relative to

the final schedule. At $T = 1.0$, the model executed 74 of the 106 gates before failing. All other models failed to generate valid schedules on this architecture. Nevertheless, partial progress was observed: Qwen-14B executed up to 52 gates, Qwen-4B up to 33 gates, and Gemma at $T = 1.0$ 16 gates, while Gemma at $T = 0.7$ and DeepSeek failed at an early stage.

Consistent with the results before, performance on the four-way junction architecture degraded as the number of qubits increased. For the circuit *mini_alu_305*, no model generated a valid schedule. LLaMA executed up to 48 gates before failing, whereas both Qwen models and Gemma executed approximately 15 gates. DeepSeek performed worst, failing to execute even a single gate. Excluding DeepSeek, these results indicate that limited progress remains possible for 10-qubit circuits, although complete schedules cannot be reliably generated.

For the circuit *cnt3-5_179*, no model produced a valid schedule, and the number of executed gates before failure further decreased compared to *mini_alu_305*. LLaMA executed 16 gates at $T = 1.0$ and 12 gates at $T = 0.7$ before failing, while all other models failed after executing between four and nine gates. These results further highlight that shuttling schedule generation becomes increasingly challenging as the number of qubits grows.

Overall, our results show that fine-tuned LLMs can generate valid shuttling schedules and can, in some cases, outperform standard heuristics. However, producing complete schedules becomes increasingly challenging with the width and depth of the algorithm. Models may enter invalid states, requiring retries that substantially inflate token counts without contributing to the final output. Generalization to previously unseen architectures remains limited. Across all experiments, LLaMA demonstrated the most stable performance, whereas Qwen, DeepSeek, and Gemma failed more frequent and at earlier stages as circuit size increased. When comparing the both Qwen models, it can be noticed that the smaller model with 4 billion parameters produced better results than the larger model with 14 billion parameters. This indicates, together with LLaMA which is with 3 billion parameters the smallest model we tested, that smaller models can be better adapted to shuttling schedule generation than larger ones.

5 Conclusion and Outlook

We have presented a shuttling compiler for trapped-ion quantum computers based on large language models (LLMs). We fine-tuned several LLMs on datasets derived from shuttling schedules generated by classical compilers for linear and branched one-dimensional trap architectures and evaluated them on circuits of varying sizes. For small circuits on both linear and junction layouts, the models were able to generate

valid schedules and in some cases even required fewer operations as compared to the standard heuristics [17, 20].

To improve the capabilities of LLM-compilers, we plan to enhance the training pipeline in two stages: first using Direct Preference Optimization (DPO) [78], and later using Gradient Regularized Policy Optimization (GRPO) [79]. Applying DPO requires generating multiple candidate shuttling operations at each step so that the model can learn which alternatives are preferable. As discussed in Sec. 3.3, the schedule with the lowest number of operations cannot always be used as the preferred example, since following it naively may lead the model into local minima that require additional operations to escape. Instead, DPO could help the model identify invalid operations by consistently deprioritizing them. To refine this further, a lookahead strategy would be needed: for each valid candidate, the shuttlings for a certain number of next gates must be computed to determine which initial choice leads to the lowest overall number of operations. While the runtime of this approach grows exponential, it provides valuable multi-step supervision.

Building on this, GRPO offers a framework for reinforcement learning with human feedback (RLHF) [80]. This would require a continuous reward function that penalizes invalid schedules and rewards valid schedules with fewer operations, again ideally using a lookahead-based evaluation. Due to the large number of shuttling generations needed for DPO and the additional computational overhead of GRPO, scaling these methods will require access to more GPUs than the eight H100 GPUs available for the present work.

Overall, our work establishes the first LLM-based shuttling compilers for trapped-ion quantum computers and may paving a way to extend performance and reliability.

Acknowledgments

We acknowledge funding by the German Federal Ministry of Research, Technology and Space (BMFTR) within the project IQuAn, ATIQ and SYNQ, and the DFG SPP2514. We thank the data center (ZDV) of the Johannes Gutenberg University for the use of their Mogon NHR and Mogon KI clusters for evaluating our LLMs.

References

[1] D. Kielpinski, C. Monroe, and D. J. Wineland. “Architecture for a large-scale ion-trap quantum computer”. *Nature* **417**, 709–711 (2002).

[2] V. Kaushal, B. Lekitsch, A. Stahl, J. Hilder, D. Pijn, C. Schmiegelow, A. Bermudez, M. Müller, F. Schmidt-Kaler, and U. Poschinger. “Shuttling-based trapped-ion quantum information processing”. *AVS Quantum Sci.* **2**, 014101 (2020). [arXiv:1912.04712](https://arxiv.org/abs/1912.04712).

[3] J. M. Pino, J. M. Dreiling, C. Figgatt, J. P. Gaebler, S. A. Moses, M. S. Allman, C. H. Baldwin, M. Foss-Feig, D. Hayes, K. Mayer, C. Ryan-Anderson, and B. Neyenhuis. “Demonstration of the trapped-ion quantum CCD computer architecture”. *Nature* **592**, 209–213 (2021). [arXiv:2003.01293](https://arxiv.org/abs/2003.01293).

[4] Prakash Murali, Dripto M. Debroy, Kenneth R. Brown, and Margaret Martonosi. “Architecting Noisy Intermediate-Scale Trapped Ion Quantum Computers”. In ACM/IEEE 47th Annu. Int. Symp. Comput. Archit. (ISCA). Pages 529–542. Virtual Event (May 30–June 3, 2020). IEEE. [arXiv:2004.04706](https://arxiv.org/abs/2004.04706).

[5] S. A. Moses, C. H. Baldwin, et al. “A Race-Track Trapped-Ion Quantum Processor”. *Phys. Rev. X* **13**, 041052 (2023). [arXiv:2305.03828](https://arxiv.org/abs/2305.03828).

[6] Stephan Schulz, Ulrich Poschinger, Kilian Singer, and Ferdinand Schmidt-Kaler. “Optimization of segmented linear Paul traps and transport of stored particles”. *Fortschr. Phys.* **54**, 648–665 (2006). [arXiv:quant-ph/0607217](https://arxiv.org/abs/quant-ph/0607217).

[7] Tobias Schmale, Bence Temesi, Alakesh Baishya, Nicolas Pulido-Mateo, Ludwig Krinner, Timko Dubielzig, Christian Ospelkaus, Hendrik Weimer, and Daniel Borcherding. “Backend compiler phases for trapped-ion quantum computers”. In IEEE Int. Conf. Quantum Softw. (QSW). Pages 32–37. Barcelona, Spain (July 10–16, 2022). IEEE. [arXiv:2206.00544](https://arxiv.org/abs/2206.00544).

[8] Anthony Ransford et al. “Helios: A 98-qubit trapped-ion quantum computer” (2025). [arXiv:2511.05465](https://arxiv.org/abs/2511.05465).

[9] R. Bowler, J. Gaebler, Y. Lin, T. R. Tan, D. Hanneke, J. D. Jost, J. P. Home, D. Leibfried, and D. J. Wineland. “Coherent Diabatic Ion Transport and Separation in a Multizone Trap Array”. *Phys. Rev. Lett.* **109**, 080502 (2012). [arXiv:1206.0780](https://arxiv.org/abs/1206.0780).

[10] Minjae Lee, Junho Jeong, Yunjae Park, Changhyun Jung, Taehyun Kim, and Dong-il Cho. “Ion shuttling method for long-range shuttling of trapped ions in MEMS-fabricated ion traps”. *Jpn. J. Appl. Phys.* **60**, 027004 (2021).

[11] W. K. Hensinger, S. Olmschenk, D. Stick, D. Hucul, M. Yeo, M. Acton, L. Deslauriers, J. Rabchuk, and C. Monroe. “T-junction ion trap array for two-dimensional ion shuttling, storage, and manipulation”. *Appl. Phys. Lett.* **88**, 034101 (2006). [arXiv:quant-ph/0508097](https://arxiv.org/abs/quant-ph/0508097).

[12] R. B. Blakestad, C. Ospelkaus, A.P. VanDevender, J.M. Amini, J. Britton, D. Leibfried,

and D.J. Wineland. “High-Fidelity Transport of Trapped-Ion Qubits through an X-Junction Trap Array”. *Phys. Rev. Lett.* **102**, 153002 (2009). [arXiv:0901.0533](#).

[13] Kenneth Wright, Jason M. Amini, Daniel L. Faircloth, Curtis Volin, S. Charles Doret, Harley Hayden, C.-S. Pai, David W. Landgren, Douglas Denison, Tyler Killian, Richard E. Slusher, and Alexa W. Harter. “Reliable transport through a microfabricated X-junction surface-electrode ion trap”. *New J. Phys.* **15**, 033004 (2013). [arXiv:1210.3655](#).

[14] G. Shu, G. Vittorini, A. Buikema, C. S. Nichols, C. Volin, D. Stick, and Kenneth R. Brown. “Heating rates and ion-motion control in a Y-junction surface-electrode trap”. *Phys. Rev. A* **89**, 062308 (2014).

[15] Bjoern Lekitsch, Sebastian Weidt, Austin G. Fowler, Klaus Mølmer, Simon J. Devitt, Christof Wunderlich, and Winfried K. Hensinger. “Blueprint for a microwave trapped ion quantum computer”. *Sci. Adv.* **3**, e1601540 (2017). [arXiv:1508.00420](#).

[16] Janine Hilder, Daniel Pijn, Oleksiy Onishchenko, Alexander Stahl, Maximilian Orth, Björn Lekitsch, Andrea Rodriguez-Blanco, Markus Müller, Ferdinand Schmidt-Kaler, and Ulrich Poschinger. “Fault-Tolerant Parity Readout on a Shuttling-Based Trapped-Ion Quantum Computer”. *Phys. Rev. X* **12**, 011032 (2022). [arXiv:2107.06368](#).

[17] Janis Wagner. “Automated generation of shuttling schedules for a scalable trapped-ion quantum processor”. M.sc. thesis. Institute of Computer Science, Johannes Gutenberg Univ. Mainz, Germany (2022).

[18] Jonathan Durandau, Janis Wagner, Frédéric Mailhot, Charles-Antoine Brunet, Ferdinand Schmidt-Kaler, Ulrich Poschinger, and Yves Bérubé-Lauzière. “Automated Generation of Shuttling Sequences for a Linear Segmented Ion Trap Quantum Computer”. *Quantum* **7**, 1175 (2023). [arXiv:2208.04881](#).

[19] Che-Ming Chang, Jie-Hong Roland Jiang, Dah-Wei Chiou, Ting Hsu, and Guin-Dar Lin. “Quantum circuit compilation for trapped-ion processors with the drive-through architecture”. *IEEE Trans. Quantum Eng. (TQE)* **6**, 1–14 (2025).

[20] Fabian Kreppel, Christian Melzer, Janis Wagner, Janine Hilder, Ulrich Poschinger, Ferdinand Schmidt-Kaler, and André Brinkmann. “Shuttling compiler for a Trapped-Ion Quantum Computer Architecture with Junctions”. In *IEEE Int. Conf. Quantum Comput. Eng. (QCE)*. **Volume 1**, pages 1065–1076. Montreal, Canada (Sept. 15–20, 2024). IEEE.

[21] Mark Webber, Steven Herbert, Sebastian Weidt, and Winfried K. Hensinger. “Efficient Qubit Routing for a Globally Connected Trapped Ion Quantum Computer”. *Adv. Quantum Technol.* **3**, 2000027 (2020). [arXiv:2002.12782](#).

[22] Weining Dai, Kevin A. Brown, and Thomas G. Robertazzi. “Advanced Shuttle Strategies for Parallel QCCD Architectures”. *IEEE Trans. Quantum Eng. (TQE)* **5**, 1–18 (2024).

[23] Daniel Schoenberger, Stefan Hillmich, Matthias Brandl, and Robert Wille. “Shuttling for Scalable Trapped-Ion Quantum Computers”. *IEEE Trans. Comp.-Aided Des. Integ. Cir. Sys.* **44**, 2144–2155 (2025). [arXiv:2402.14065](#).

[24] Daniel Schoenberger, Janine Hilder, Ferdinand Schmidt-Kaler, and Robert Wille. “Shuttling for Trapped-Ion Quantum Computers with Embedded Processing Zones”. In *IEEE Int. Conf. Quantum Softw. (QSW)*. Pages 123–129. Helsinki, Finland (July 7–12, 2025). IEEE.

[25] Daniel Schoenberger and Robert Wille. “Orchestrating Multi-Zone Shuttling in Trapped-Ion Quantum Computers”. In *IEEE Int. Conf. Quantum Comput. Eng. (QCE)*. **Volume 1**, pages 1069–1075. Albuquerque, NM, USA (Aug. 31–Sept. 5, 2025). IEEE. [arXiv:2505.07928](#).

[26] Tom B. Brown et al. “Language models are few-shot learners”. In *34th Int. Conf. Neural Inf. Process. Syst. (NeurIPS)*. Pages 1877–1901. Virtual event (Dec. 6–12, 2020). Curran Associates Inc. [arXiv:2005.14165](#).

[27] Meta AI (2024). code: [meta-llama/llama-models](#) commit:4a9ff6a.

[28] Qwen Team. “Qwen3 Technical Report” (2025). [arXiv:2505.09388](#).

[29] DeepSeek-AI. “DeepSeek LLM: Scaling Open-Source Language Models with Longtermism” (2024). [arXiv:2401.02954](#).

[30] Gemma Team. “Gemma 3 Technical Report” (2025). [arXiv:2503.19786](#).

[31] Alexandru Paler, Lucian Sasu, Adrian-Cătălin Florea, and Răzvan Andonie. “Machine Learning Optimization of Quantum Circuit Layouts”. *ACM Trans. Quantum Comput. (TQC)* **4**, 12:1–12:25 (2023). [arXiv:2007.14608](#).

[32] Matteo G. Pozzi, Steven J. Herbert, Akash Sengupta, and Robert D. Mullins. “Using Reinforcement Learning to Perform Qubit Routing in Quantum Compilers”. *ACM Trans. Quantum Comput. (TQC)* **3**, 10:1–10:25 (2022). [arXiv:2007.15957](#).

[33] Hongxiang Fan, Ce Guo, and Wayne Luk. “Optimizing quantum circuit placement via machine learning”. In *59th ACM/IEEE Des. Automat.*

Conf. (DAC). *Pages 19–24*. San Francisco, CA, USA (July 10–14, 2022). ACM.

[34] Gonçalo Pascoal, João Paulo Fernandes, and Rui Abreu. “Deep Reinforcement Learning Strategies for Noise-Adaptive Qubit Routing”. In IEEE Int. Conf. Quantum Softw. (QSW). *Pages 146–156*. Shenzhen, China (July 7–13, 2024). IEEE.

[35] Wei Tang, Yiheng Duan, Yaroslav Kharkov, Rasool Fakoor, Eric Kessler, and Yunong Shi. “AlphaRouter: Quantum Circuit Routing with Reinforcement Learning and Tree Search”. In IEEE Int. Conf. Quantum Comput. Eng. (QCE). *Volume 1, pages 930–940*. Montreal, Canada (Sept. 15–20, 2024). IEEE. [arXiv:2410.05115](https://arxiv.org/abs/2410.05115).

[36] Animesh Sinha, Utkarsh Azad, and Harjinder Singh. “Qubit Routing Using Graph Neural Network Aided Monte Carlo Tree Search”. In 36th AAAI Conf. Artif. Intell. *Pages 9935–9943*. Virtual Event (Feb. 22–Mar. 1, 2022). AAAI. [arXiv:2104.01992](https://arxiv.org/abs/2104.01992).

[37] Enrico Russo, Maurizio Palesi, Davide Patti, Giuseppe Ascia, and Vincenzo Catania. “Optimizing Qubit Assignment in Modular Quantum Systems via Attention-Based Deep Reinforcement Learning”. In Des. Automat. Test Europe Conf. (DATE). *Pages 1–7*. Lyon, France (Mar. 31–Apr. 2, 2025). IEEE. [arXiv:2406.11452](https://arxiv.org/abs/2406.11452).

[38] Sokea Sang, Leanghok Hour, and Youngsun Han. “Learning-Optimized Qubit Mapping and Reuse to Minimize Inter-Core Communication in Modular Quantum Architectures” (2025). [arXiv:2506.09323](https://arxiv.org/abs/2506.09323).

[39] Atiye Zeynali and Zahra Bakhshi. “Noise-Adaptive Quantum Circuit Mapping for Multi-Chip NISQ Systems via Deep Reinforcement Learning” (2025). [arXiv:2511.18079](https://arxiv.org/abs/2511.18079).

[40] Daniele Cuomo, Marcello Caleffi, Kevin Kr-slich, Filippo Tramonto, Gabriele Agliardi, Enrico Prati, and Angela Sara Cacciapuoti. “Optimized Compiler for Distributed Quantum Computing”. *ACM Trans. Quantum Comput. (TQC)* **4**, 15:1–15:29 (2023). [arXiv:2112.14139](https://arxiv.org/abs/2112.14139).

[41] Pau Escofet, Anabel Ovide, Medina Bandic, Luise Prielinger, Hans van Someren, Sebastian Feld, Eduard Alarcon, Sergi Abadal, and Carmen Almudever. “Revisiting the Mapping of Quantum Circuits: Entering the Multi-core Era”. *ACM Trans. Quantum Comput. (TQC)* **6**, 4:1–4:26 (2025). [arXiv:2403.17205](https://arxiv.org/abs/2403.17205).

[42] Ranjani Sundaram, Himanshu Gupta, and CR Ramakrishnan. “DQC-QR: Distributing and Routing Quantum Circuits with Minimum Execution Time”. *ACM Trans. Quantum Comput. (TQC)* **6**, 30:1–30:26 (2025). [arXiv:2405.07499](https://arxiv.org/abs/2405.07499).

[43] Robert Wille, Rod Van Meter, and Yehuda Naveh. “IBM’s Qiskit Tool Chain: Working with and Developing for Real Quantum Computers”. In Des. Automat. Test Europe Conf. Exhib. (DATE). *Pages 1234–1240*. Florence, Italy (Mar. 25–29, 2019). IEEE.

[44] Seyon Sivarajah, Silas Dilkes, Alexander Cowtan, Will Simmons, Alec Edgington, and Ross Duncan. “ $t|ket\rangle$: a retargetable compiler for NISQ devices”. *Quantum Sci. Technol.* **6**, 014003 (2020). [arXiv:2003.10611](https://arxiv.org/abs/2003.10611).

[45] Cirq Developers. “Cirq”. *Zenodo*. (2025).

[46] Ville Bergholm et al. “PennyLane: Automatic differentiation of hybrid quantum-classical computations” (2022). [arXiv:1811.04968](https://arxiv.org/abs/1811.04968).

[47] Daniel Schoenberger, Stefan Hillmich, Matthias Brandl, and Robert Wille. “Using Boolean Satisfiability for Exact Shuttling in Trapped-Ion Quantum Computers”. In 29th Asia South Pacific Des. Automat. Conf. (ASP-DAC). *Pages 127–133*. Incheon, Republic of Korea (Jan. 22–25, 2024). IEEE. [arXiv:2311.03454](https://arxiv.org/abs/2311.03454).

[48] Abdullah Ash-Saki, Rasit Onur Topaloglu, and Swaroop Ghosh. “Muzzle the Shuttle: Efficient Compilation for Multi-Trap Trapped-Ion Quantum Computers”. In Des. Automat. Test Europe Conf. Exhib. (DATE). *Pages 322–327*. Antwerp, Belgium (Mar. 14–23, 2022). IEEE. [arXiv:2111.07961](https://arxiv.org/abs/2111.07961).

[49] Xian Wu, Chenghong Zhu, Jingbo Wang, and Xin Wang. “MUSS-TI: Multi-level Shuttle Scheduling for Large-Scale Entanglement Module Linked Trapped-Ion”. In 58th IEEE/ACM Int. Symp. Microarchit. (MICRO). *Pages 749–763*. Seoul, Republic of Korea (Oct. 18–22, 2025). ACM. [arXiv:2509.25988](https://arxiv.org/abs/2509.25988).

[50] Rohan Taori, Ishaan Gulrajani, Tianyi Zhang, Yann Dubois, Xuechen Li, Carlos Guestrin, Percy Liang, and Tatsunori B. Hashimoto (2023). code: tatsu-lab/stanford_alpaca commit: [761dc5b](https://github.com/tatsu-lab/stanford_alpaca/commit/761dc5b).

[51] Arezoo Mokhberi, Roman Schmied, and Stefan Willitsch. “Optimised surface-electrode ion-trap junctions for experiments with cold molecular ions”. *New J. Phys.* **19**, 043023 (2017). [arXiv:1701.06408](https://arxiv.org/abs/1701.06408).

[52] Thomas Wolf et al. “Transformers: State-of-the-Art Natural Language Processing”. In Conf. Empirical Methods Natural Lang. Process.: Syst. Demonstrations. *Pages 38–45*. Online Event (Nov. 16–20, 2020). ACL. [arXiv:1910.03771](https://arxiv.org/abs/1910.03771).

[53] Axolotl maintainers and contributors. “Axolotl: Open Source LLM Post-Training” (2023).

[54] Edward J. Hu, Yelong Shen, Phillip Wallis, Zeyuan Allen-Zhu, Yuanzhi Li, Shean Wang, Lu Wang, and Weizhu Chen. “LoRA: Low-Rank Adaptation of Large Language Models”. In 10th Int. Conf. Learn. Representations (ICLR). *Pages 1–13*. Virtual event (Apr. 25–29, 2022). OpenReview. [arXiv:2106.09685](#).

[55] Tim Dettmers, Artidoro Pagnoni, Ari Holtzman, and Luke Zettlemoyer. “QLoRA: Efficient Finetuning of Quantized LLMs”. In 37th Int. Conf. Neural Inf. Process. Syst. (NeurIPS). *Pages 10088–10115*. New Orleans, LA, USA (Dec. 10–16, 2023). Curran Associates Inc. [arXiv:2305.14314](#).

[56] Achintya Kundu, Rhui Dih Lee, Laura Wynter, Raghu Kiran Ganti, and Mayank Mishra. “Enhancing Training Efficiency Using Packing with Flash Attention” (2024). [arXiv:2407.09105](#).

[57] Tri Dao. “FlashAttention-2: Faster Attention with Better Parallelism and Work Partitioning”. In 12th Int. Conf. Learn. Representations (ICLR). *Pages 1–14*. Vienna, Austria (May 7–11, 2024). OpenReview. [arXiv:2307.08691](#).

[58] Deepak Narayanan, Mohammad Shoeybi, Jared Casper, Patrick LeGresley, Mostofa Patwary, Vijay Korthikanti, Dmitri Vainbrand, Prethvi Kashinkunti, Julie Bernauer, Bryan Catanzaro, Amar Phanishayee, and Matei Zaharia. “Efficient Large-Scale Language Model Training on GPU Clusters Using Megatron-LM”. In Int. Conf. High Perform. Comput., Netw., Storage Anal. (SC21). *Pages 58:1–58:15*. St. Louis, MO, USA (Nov. 14–19, 2021). ACM. [arXiv:2104.04473](#).

[59] Jeff Rasley, Samyam Rajbhandari, Olatunji Ruwase, and Yuxiong He. “DeepSpeed: System Optimizations Enable Training Deep Learning Models with Over 100 Billion Parameters”. In 26th ACM SIGKDD Int. Conf. Knowl. Discovery & Data Mining. *Pages 3505–3506*. Virtual Event (July 6–10, 2020). ACM.

[60] Samyam Rajbhandari, Jeff Rasley, Olatunji Ruwase, and Yuxiong He. “ZeRO: Memory optimizations Toward Training Trillion Parameter Models”. In Int. Conf. High Perform. Comput., Netw., Storage Anal. (SC20). *Pages 20:1–20:16*. Atlanta, GA, USA (Nov. 9–19, 2020). IEEE. [arXiv:1910.02054](#).

[61] Mohammad Shoeybi, Mostofa Patwary, Raul Puri, Jared Casper Patrick LeGresley, and Bryan Catanzaro. “Megatron-LM: Training Multi-Billion Parameter Language Models Using Model parallelism” (2019). [arXiv:1909.08053](#).

[62] Jie Ren, Samyam Rajbhandari, Reza Yazdani Aminabadi, Olatunji Ruwase, Shuangyan Yang, Minjia Zhang, Dong Li, and Yuxiong He. “ZeRO-Offload: Democratizing Billion-Scale Model Training”. In USENIX Annu. Tech. Conf. (USENIX ATC 21). *Pages 551–564*. Virtual event (July 14–16, 2021). USENIX Association. [arXiv:2101.06840](#).

[63] Hao Liu, Matei Zaharia, and Pieter Abbeel. “RingAttention with Blockwise Transformers for Near-Infinite Context”. In 12th Int. Conf. Learn. Representations (ICLR). *Pages 1–17*. Vienna, Austria (May 7–11, 2024). OpenReview. [arXiv:2310.01889](#).

[64] Ilya Loshchilov and Frank Hutter. “Decoupled Weight Decay Regularization”. In 7th Int. Conf. Learn. Representations (ICLR). *Pages 1–18*. New Orleans, LA, USA (May 6–9, 2019). OpenReview. [arXiv:1711.05101](#).

[65] Woosuk Kwon, Zhuohan Li, Siyuan Zhuang, Ying Sheng, Lianmin Zheng, Cody Hao Yu, Joseph E. Gonzalez, Hao Zhang, and Ion Stoica. “Efficient Memory Management for Large Language Model Serving with Page-dAttention”. In 29th ACM Symp. Operating Syst. Princ. (SOSP). *Pages 611–626*. Koblenz, Germany (Oct. 23–26, 2023). ACM. [arXiv:2309.06180](#).

[66] Andrew W. Cross, Lev S. Bishop, John A. Smolin, and Jay M. Gambetta. “Open Quantum Assembly Language” (2017). [arXiv:1707.03429](#).

[67] Andrew Cross, Ali Javadi-Abhari, Thomas Alexander, Niel De Beaudrap, Lev S. Bishop, Steven Heidel, Colm A. Ryan, Prasahnt Sivarajah, John Smolin, Jay M. Gambetta, and Blake R. Johnson. “OpenQASM 3: A Broader and Deeper Quantum Assembly Language”. *ACM Trans. Quantum Comput. (TQC) 3, 12:1–12:50* (2022). [arXiv:2104.14722](#).

[68] Fabian Kreppel, Christian Melzer, Diego Olvera Millán, Janis Wagner, Janine Hilder, Ulrich Poschinger, Ferdinand Schmidt-Kaler, and André Brinkmann. “Quantum Circuit Compiler for a Shuttling-Based Trapped-Ion Quantum Computer”. *Quantum 7, 1176* (2023). [arXiv:2207.01964](#).

[69] DeepSeek-AI. “DeepSeek-V3 Technical Report” (2024). [arXiv:2412.19437](#).

[70] Daya Guo, Dejian Yang, Haowei Zhang, et al. “DeepSeek-R1 incentivizes reasoning in LLMs through reinforcement learning”. *Nature 645, 633–638* (2025).

[71] Meta AI (2025). code: [meta-llama/llama-models commit:038acb9](#).

[72] OpenAI. “gpt-oss-120b & gpt-oss-20b Model Card” (2025). [arXiv:2508.10925](#).

[73] Yanli Zhao et al. “PyTorch FSDP: Experiences on Scaling Fully Sharded Data Parallel” (2023). [arXiv:2304.11277](#).

[74] Xiangzhen Zhou (2019). code: [Ben-Zhou1991/circuittransform](#) commit:8e6e5b1.

[75] Xiangzhen Zhou, Sanjiang Li, and Yuan Feng. “Quantum Circuit Transformation Based on Simulated Annealing and Heuristic Search”. *IEEE Trans. Comp.-Aided Des. Integ. Cir. Sys.* **39**, 4683–4694 (2020). [arXiv:1908.08853](#).

[76] Alexander Cowtan, Silas Dilkes, Ross Duncan, Alexandre Krajenbrink, Will Simmons, and Seyon Sivarajah. “On the Qubit Routing Problem”. In 14th Conf. Theory Quantum Comput. Commun. Cryptography (TQC). Pages 5:1–5:32. Univ. of Maryland, College Park, MD, USA (June 3–5, 2019). Schloss Dagstuhl – Leibniz-Zentrum für Informatik. [arXiv:1902.08091](#).

[77] Ander Artola Velasco, Stratis Tsirtsis, Nas-taran Okati, and Manuel Gomez-Rodriguez. “Is Your LLM Overcharging You? Tokenization, Transparency, and Incentives” (2025). [arXiv:2505.21627](#).

[78] Rafael Rafailov, Archit Sharma, Eric Mitchell, Stefano Ermon, Christopher D. Manning, and Chelsea Finn. “Direct Preference Optimization: Your Language Model is Secretly a Reward Model”. In 34th Int. Conf. Neural Inf. Process. Syst. (NeurIPS). Pages 53728–53741. New Orleans, LA, USA (Dec. 10–16, 2023). Curran Associates Inc. [arXiv:2305.18290](#).

[79] OpenAI. “OpenAI o1 System Card” (2024). [arXiv:2412.16720](#).

[80] Paul F. Christiano, Jan Leike, Tom B. Brown, Miljan Martic, Shane Legg, and Dario Amodei. “Deep reinforcement learning from human preferences”. In 31th Int. Conf. Neural Inf. Process. Syst. (NIPS). Pages 4302—4310. Long Beach, CA, USA (Dec. 4–9, 2017). Curran Associates Inc. [arXiv:1706.03741](#).